PHYSICAL REVIEW D **73,** 094503 (2006)

Nucleon structure functions with domain wall fermions

K. Orginos,[1] T. Blum,[2,3] and S. Ohta[4,5,2]

[1]*CTP/LNS, Room 6-304, Massachusetts Institute of Technology, 77 Massachusetts Ave., Cambridge, Massachusetts 02139-4307, USA*
[2]*RIKEN-BNL Research Center, Brookhaven National Laboratory, Upton, New York 11973, USA*
[3]*Physics Department, University of Connecticut, Storrs, Connecticut 06269-3046, USA*
[4]*Institute for Particle and Nuclear Studies, KEK, Tsukuba, Ibaraki, 305-0801, Japan*
[5]*The Graduate University for Advanced Studies (SOKENDAI), Tsukuba, Ibaraki 305-0801, Japan*

(Received 2 June 2005; published 12 May 2006)

We present a quenched lattice QCD calculation of the first few moments of the polarized and unpolarized structure functions of the nucleon. Our calculations are done using domain wall fermions and the DBW2 gauge action with inverse lattice spacing $a^{-1} \approx 1.3$ GeV, physical volume $V \approx (2.4 \text{ fm})^3$, and light quark masses down to about $1/4$ the strange quark mass ($m_\pi \approx 400$ MeV). Values of the individual moments are found to be significantly larger than experiment, as in past lattice calculations, but interestingly the chiral symmetry of domain wall fermions allows for a precise determination of the ratio of the flavor nonsinglet momentum fraction to the helicity distribution, $\langle x \rangle_{u-d}/\langle x \rangle_{\Delta u - \Delta_d}$, which is in very good agreement with experiment. We discuss the implications of this result. Next, we show that the chiral symmetry of domain wall fermions is useful in eliminating mixing of power divergent lower dimensional operators with twist-3 operators. Finally, we compute the isovector tensor charge at renormalization scale $\mu = 2$ GeV in the $\overline{MS}$ scheme, $\langle 1 \rangle_{\delta u - \delta d} = 1.192(30)$, where the error is the statistical error only.

DOI: 10.1103/PhysRevD.73.094503 PACS numbers: 11.15.Ha, 12.38.−t, 12.38.Aw, 12.38.Gc

I. INTRODUCTION

Quantum Chromodynamics (QCD) is the theory describing the strong interactions, and hence it is responsible for the properties of hadronic matter. Unlike Quantum Electrodynamics (QED), its nonperturbative nature, or strong coupling constant, makes it difficult to understand the low energy content of the theory. The lattice formulation of QCD provides both a nonperturbative way of defining the theory and a very powerful tool to calculate its properties.

Deep inelastic scattering of leptons on nucleons has been the basic experimental tool in probing QCD [1–12]. These experiments have given rise to the parton model and, through extensive fits, have indirectly allowed the measurement of the parton distribution functions, the basic structural blueprint for hadrons. Connecting these experiments to the underlying theory of QCD is an important theoretical endeavor. During the last few years lattice computations have provided many interesting results for nucleon matrix elements [13–24], in both quenched and full QCD. These calculations provide first-principles values for the moments of structure functions at leading twist. One of the major unresolved issues in these previous calculations is the approach to the chiral limit; computational limitations have restricted calculations to relatively large quark masses, introducing ambiguities in the extrapolation to the chiral limit. Furthermore, values calculated using the lattice regularization have significantly overestimated results from fits to the experimental data [13,15,25], leading to suggestions in the literature that strong suppression in the chiral limit is required to resolve the problem [26].

We address this question with a calculation using domain wall fermions [27–29]. Preliminary results have been given in [17,19,20]. The use of domain wall fermions allows us to examine the source of several systematic errors. Chiral symmetry at nonzero lattice spacing minimizes discretization errors, $O(a^2)$ in this case. Thus we work with relatively coarse lattice spacing, $a \approx 0.15$ fm, and therefore larger physical volume $L \approx 2.4$ fm. This means calculations with light quark masses will not suffer unduly large finite size corrections. In this study the lightest quark mass is roughly $1/4$ of the strange quark mass, as light as has been used in nucleon structure calculations. Chiral symmetry makes the renormalization properties of operators simpler since there is less mixing with unwanted operators. Here operators are nonperturbatively renormalized, reducing a significant source of systematic error. We have also chosen to use the DBW2 gauge as it substantially reduces the already small explicit chiral symmetry breaking for domain wall fermions with finite extra fifth dimension [30,31].

The remainder of this paper is organized as follows. In Sec. II we briefly recall the polarized and unpolarized structure functions of the nucleon arising from deep inelastic scattering and the operators that arise from their operator product expansions. The lattice transcription of operators and correlation functions are described in Sec. III. Perturbative and nonperturbative aspects of operator renormalization are discussed in Sec. IV. Details of the numerical simulation are given in Sec. V. Sec. VI, containing the presentation and discussion of results, is the main part of the paper. We summarize the present study and comment on future calculations in Sec. VII.

II. NUCLEON STRUCTURE FUNCTIONS

The cross-section for deep inelastic scattering of leptons on a nucleon target is given by the square of the matrix element for an initial state lepton-proton pair to scatter to a final state of a lepton and hadrons. After summing over all possible final states, the square of the matrix element is computed using the optical theorem which relates the summed, squared, matrix element to the forward matrix element between nucleon states of the product of two electromagnetic currents.

$$\sigma \sim L^{\mu\nu} W_{\mu\nu}, \tag{1}$$

$$W_{\mu\nu} = i \int d^4x e^{iqx} \langle N | T\{J^\mu(x), J^\nu(0)\} | N \rangle, \tag{2}$$

where $L^{\mu\nu}$ and $W_{\mu\nu}$ are leptonic and hadronic tensors, respectively, and q is the spacelike four-momentum transfered to the nucleon by scattering off the electron through a virtual photon. The leptonic part is handled in perturbation theory since the QED coupling constant is small; the hadronic part, however must be treated nonperturbatively which is the focus of this paper.

The hadronic tensor is conveniently split, $W_{\mu\nu} = W^{[\mu\nu]} + W^{\{\mu\nu\}}$. The symmetric piece defines the unpolarized, or spin-average structure functions F_1 and F_2 (and F_3 if we consider neutrino scattering).

$$W^{\{\mu\nu\}}(x, Q^2) = \left(-g^{\mu\nu} + \frac{q^\mu q^\nu}{q^2}\right) F_1(x, Q^2) + \left(p^\mu - \frac{\nu}{q^2} q^\mu\right)\left(p^\nu - \frac{\nu}{q^2} q^\nu\right) \frac{F_2(x, Q^2)}{\nu},$$

while the antisymmetric piece defines the polarized structure functions g_1 and g_2

$$W^{[\mu\nu]}(x, Q^2) = i\epsilon^{\mu\nu\rho\sigma} q_\rho \left(\frac{s_\sigma}{\nu} (g_1(x, Q^2) + g_2(x, Q^2)) - \frac{q \cdot s p_\sigma}{\nu^2} g_2(x, Q^2) \right). \tag{3}$$

p_μ and s_μ are the nucleon momentum and spin four-vectors, $\nu = q \cdot p$, $s^2 = -m_N^2$ is our choice of normalization, $x = Q^2/2\nu$, $Q^2 = -q^2 > 0$ and m_N is the nucleon mass.

At the leading twist in the operator product expansion of the two electromagnetic currents in Eq. (2), the moments of the structure functions can be factorized, at scale μ, into hard perturbative contributions (the Wilson coefficients) and low energy matrix elements of local gauge invariant operators. Adopting the notation of [32],

$$\begin{aligned}
2\int_0^1 dx x^{n-1} F_1(x, Q^2) &= \sum_{q=u,d} c_{1,n}^{(q)}(\mu^2/Q^2, g(\mu)) v_n^{(q)}(\mu), \\
\int_0^1 dx x^{n-2} F_2(x, Q^2) &= \sum_{q=u,d} c_{2,n}^{(q)}(\mu^2/Q^2, g(\mu)) v_n^{(q)}(\mu), \\
2\int_0^1 dx x^{n} g_1(x, Q^2) &= \frac{1}{2} \sum_{q=u,d} e_{1,n}^{(q)}(\mu^2/Q^2, g(\mu)) a_n^{(q)}(\mu), \\
2\int_0^1 dx x^{n} g_2(x, Q^2) &= \frac{1}{2} \frac{n}{n+1} \sum_{q=u,d} [e_{2,n}^{(q)}(\mu^2/Q^2, g(\mu)) d_n^{(q)}(\mu) - e_{1,n}^{(q)}(\mu^2/Q^2, g(\mu)) a_n^{(q)}(\mu)]
\end{aligned} \tag{4}$$

where $c_{i,n}^{(q)}$, $e_{i,n}^{(q)}$ are the Wilson coefficients and $v_n^{(q)}(\mu)$, $a_n^{(q)}(\mu)$, $d_n^{(q)}(\mu)$ are the nonperturbative matrix elements. At the leading twist $v_n^{(q)}(\mu)$ and $a_n^{(q)}(\mu)$ are related to the parton model distribution functions $\langle x^n \rangle_q$ and $\langle x^n \rangle_{\Delta q}$:

$$\langle x^{n-1} \rangle_q = v_n^{(q)} \qquad \langle x^n \rangle_{\Delta q} = \frac{1}{2} a_n^{(q)} \tag{5}$$

To determine $v_n^{(q)}(\mu)$, $a_n^{(q)}(\mu)$ and $d_n^{(q)}(\mu)$ we need to compute nonperturbatively the following matrix elements:

$$\begin{aligned}
\frac{1}{2}\sum_s \langle p, s | \mathcal{O}^q_{\{\mu_1\mu_2\cdots\mu_n\}} | p, s \rangle &= 2 v_n^{(q)}(\mu) \times [p_{\mu_1} p_{\mu_2} \cdots p_{\mu_n} + \cdots - \text{tr}] - \langle p, s | \mathcal{O}^{5q}_{\{\sigma\mu_1\mu_2\cdots\mu_n\}} | p, s \rangle \\
&= \frac{1}{n+1} a_n^{(q)}(\mu) \times [s_\sigma p_{\mu_1} p_{\mu_2} \cdots p_{\mu_n} + \cdots - \text{tr}] \langle p, s | \mathcal{O}^{[5]q}_{[\sigma\{\mu_1]\mu_2\cdots\mu_n\}} | p, s \rangle \\
&= \frac{1}{n+1} d_n^q(\mu) \times [(s_\sigma p_{\mu_1} - s_{\mu_1} p_\sigma) p_{\mu_2} \cdots p_{\mu_n} + \cdots - \text{tr}]
\end{aligned} \tag{6}$$

{} implies symmetrization and [ ] antisymmetrization of indices. The nucleon states $|p, s\rangle$ are normalized so that $\langle p, s | p', s' \rangle = (2\pi)^3 2E(p) \delta(p - p') \delta_{s,s'}$. The operators $\mathcal{O}$ are

$$\mathcal{O}^{q}_{\mu_1\mu_2\cdots\mu_n} = \left(\frac{i}{2}\right)^{n-1} \bar{q}\gamma_{\mu_1}\overleftrightarrow{D}_{\mu_2}\cdots\overleftrightarrow{D}_{\mu_n}q - \text{trace},$$
$$\mathcal{O}^{5q}_{\sigma\mu_1\mu_2\cdots\mu_n} = \left(\frac{i}{2}\right)^{n} \bar{q}\gamma_{\sigma}\gamma_5\overleftrightarrow{D}_{\mu_2}\cdots\overleftrightarrow{D}_{\mu_n}q - \text{trace}, \quad (7)$$

where $\overleftrightarrow{D} = \vec{D} - \overleftarrow{D}$ and $\vec{D}$, $\overleftarrow{D}$ are covariant derivatives acting on the right and the left, respectively.

In Drell-Yan processes the transversity distribution $\langle x\rangle_{\delta q}$ can be measured (for details see [33–35]). The relevant matrix element is

$$\langle p,s|\mathcal{O}^{\sigma q}_{\rho\nu\{\mu_1\mu_2\cdots\mu_n\}}|p,s\rangle = \frac{2}{m_N}\langle x^n\rangle_{\delta q}(\mu)\times[(s_\rho p_\nu - s_\nu p_\rho) \times p_{\mu_1}p_{\mu_2}\cdots p_{\mu_n} + \cdots - \text{tr}]$$

where

$$\mathcal{O}^{\sigma q}_{\rho\nu\mu_1\mu_2\cdots\mu_n} = \left(\frac{i}{2}\right)^{n} \bar{q}\gamma_5\sigma_{\rho\nu}\overleftrightarrow{D}_{\mu_1}\cdots\overleftrightarrow{D}_{\mu_n}q - \text{trace}. \quad (8)$$

III. LATTICE MATRIX ELEMENTS

The nonperturbative calculation of the matrix elements described in the previous section (structure function moments) proceeds, as do all Euclidean lattice calculations, through the computation of nucleon three- and two- point correlation functions,

$$C^{\Gamma,\mathcal{O}}_{3\,\text{pt}}(\vec{p},t,\tau) = \sum_{\alpha,\beta}\Gamma_{\alpha\beta}\langle J_\beta(\vec{p},t)\mathcal{O}(\tau)\bar{J}_\alpha(\vec{p},0)\rangle, \quad (9)$$

$$C_{2\,\text{pt}}(\vec{p},t) = \sum_{\alpha,\beta}\left(\frac{1+\gamma_4}{2}\right)_{\alpha\beta}\langle J_\beta(\vec{p},t)\bar{J}_\alpha(\vec{p},0)\rangle, \quad (10)$$

where $\bar{J}(\vec{p},0)$ and $J(\vec{p},t)$ are interpolating fields with the quantum numbers of the nucleon and definite momentum. $\Gamma_{\alpha\beta}$ is a Dirac matrix projection operator which is taken as

$$\Gamma = \frac{1+\gamma_4}{2} \quad (11)$$

for unpolarized matrix elements, and

$$\Gamma = \frac{1+\gamma_4}{2}i\gamma_5\gamma_k, \qquad (k\neq 4) \quad (12)$$

for polarized matrix elements. $\frac{1+\gamma_4}{2}$ projects out the positive parity part of the baryon propagator. For the proton a typical choice for the interpolating field is [36]

$$J_\alpha(\vec{p},t) = \sum_{\vec{x},a,b,c} e^{-i\vec{p}\cdot\vec{x}}\epsilon^{abc}[u^T_a(y_1,t)C\gamma_5 d_b(y_2,t)]u_{c,\alpha}(y_3,t) \times \phi(y_1-x)\phi(y_2-x)\phi(y_3-x) \quad (13)$$

with charge conjugation matrix $C=\gamma_4\gamma_2$, α a spinor index, and a, b, c color indices. The functions $\phi(x)$ are smearing functions that are designed to maximize the overlap of the interpolating field with the ground state of the nucleon. For the source we used $\phi(x)=1$ when x is within a box of size $R\sim 1$ fm and zero outside this box. For the sink we took a point sink, $\phi(x)=\delta(x)$. We have optimized the size of the box to maximize the overlap of the source to the ground state. This setup works well for zero spatial momentum of the proton, and since we studied only this case so far, this was all we needed to do. For nonzero momentum this smearing is not optimal; one must resort to other smearing methods such as gauge invariant Gaussian or Wuppertal smearing [13,15].

In the limit when the Euclidean time separation between all operators is large, $t\gg\tau\gg 0$, the desired matrix element between ground states dominates the correlation function,

$$C_{2pt}(\vec{p},t) = Z_N\frac{E_N(\vec{p})+m_N}{2E(\vec{p})}e^{-E_N(\vec{p})t} + \cdots$$
$$C^{\Gamma,\mathcal{O}}_{3pt}(\vec{p},t,\tau) = Z_N\sum_{\alpha,\beta,s,s'}\Gamma_{\alpha\beta}\frac{u_\alpha(p,s)\langle p,s|\mathcal{O}|p,s'\rangle\bar{u}_\beta(p,s')}{(2E(\vec{p}))^2} \times e^{-E_N(\vec{p})t} + \cdots \quad (14)$$

where $u(p,s)$ is the nucleon spinor satisfying the Dirac equation, and $\langle 0|J_\alpha(\vec{p},t)|p,s\rangle = \sqrt{Z_N}u_\alpha(p,s)$. Using Eq. (6) and (14) (or Eq. (8)) the desired matrix elements can be extracted from the ratio of three point functions to two-point functions. In practice we would like to achieve the asymptotic behavior of Eq. (14) with as small as possible t. For that reason the smeared interpolating operator J is essential. For more details on the technical aspects of the lattice calculation the reader may refer to [13,15,37,38].

The momentum fraction $\langle x\rangle_q$ carried by each valence quark in the nucleon is computed in Euclidean space by inserting into the correlation function the operator

$$\mathcal{O}^{q}_{44} = \bar{q}\left[\gamma_4\overleftrightarrow{D}_4 - \frac{1}{3}\sum_k\gamma_k\overleftrightarrow{D}_k\right]q. \quad (15)$$

$\overleftrightarrow{D}$ is the lattice covariant derivative, or difference operator,

$$\overleftrightarrow{D} = \vec{D} - \overleftarrow{D} \quad (16)$$

with

$$\vec{D}q = \frac{1}{2}[U_\mu(x)q(x+\hat{\mu}) - U^\dagger_\mu(x-\hat{\mu})q(x-\hat{\mu})]$$
$$\bar{q}\overleftarrow{D} = \frac{1}{2}[\bar{q}(x+\hat{\mu})U^\dagger_\mu(x) - \bar{q}(x-\hat{\mu})U_\mu(x-\hat{\mu})] \quad (17)$$

and q, $\bar{q}$ are the quark fields. $\mathcal{O}^q_{44}$ belongs to the $\mathbf{3^+_1}$ representation[1] of the hypercubic group H(4) and does not mix with any lower dimensional operators under renormalization [32,39]. The ratio,

[1]The representations of H(4) are denoted as $\mathbf{d^C_n}$, where $\mathbf{d}$ is the dimension of the representation, $\mathbf{C}$ is the charge conjugation and the subscript distinguishes between different representations of the same dimensionality and charge conjugation.

$$R_{\langle x\rangle_q} = \frac{C_{3\,\mathrm{pt}}^{\Gamma,\mathcal{O}_{44}^q}}{C_{2\,\mathrm{pt}}} = m_N\langle x\rangle_q, \tag{18}$$

then yields the momentum fraction.

Similarly, the helicity distribution $\langle x\rangle_{\Delta q}$ for each valence quark is computed from the operator

$$\mathcal{O}_{\{34\}}^{5q} = i\bar{q}\gamma_5[\gamma_3\overleftrightarrow{D}_4 + \gamma_4\overleftrightarrow{D}_3]q, \tag{19}$$

belonging to the $\mathbf{6_3^-}$ representation of H(4). It also does not mix with lower dimensional operators under renormalization [32,39]. The ratio yields

$$R_{\langle x\rangle_{\Delta q}} = \frac{C_{3\,\mathrm{pt}}^{\Gamma,\mathcal{O}_{\{34\}}^{5q}}}{C_{2\,\mathrm{pt}}} = m_N\langle x\rangle_{\Delta q}. \tag{20}$$

The lowest moment of the transversity, $\langle 1\rangle_{\Delta q}$, related to the tensor charge of the nucleon, is computed in Euclidean space using the operator

$$\mathcal{O}_{34}^{\sigma q} = \bar{q}\gamma_5\sigma_{34}q, \tag{21}$$

with $\sigma_{\mu\nu} = \frac{i}{2}[\gamma_\mu, \gamma_\nu]$. This operator belongs to the $\mathbf{6_1^+}$ representation of H(4) and does not mix with any lower dimensional operators under renormalization [32,39]. Again

$$R_{\langle 1\rangle_{\delta q}} = \frac{C_{3\,\mathrm{pt}}^{\Gamma,\mathcal{O}_{34}^{\sigma q}}}{C_{2\,\mathrm{pt}}} = \langle 1\rangle_{\delta q}. \tag{22}$$

Finally the twist-3 matrix element d_1 related to g_1 and g_2 is given by the operator

$$\mathcal{O}_{[34]}^{5q} = i\bar{q}\gamma_5[\gamma_3\overleftrightarrow{D}_4 - \gamma_4\overleftrightarrow{D}_3]q, \tag{23}$$

belonging to the $\mathbf{6_1^+}$ representation of H(4). $\mathcal{O}_{[34]}^{5q}$ is allowed to mix with lower dimensional operator $\mathcal{O}_{34}^{\sigma q}$ if the lattice fermions do not respect chiral symmetry. The mixing coefficient in this case is linearly divergent with the inverse lattice spacing and hence a nonperturbative subtraction is required [14]. The use of domain wall fermions eliminates this problem as first shown in [19] and in Sec. VI. d_1 is given by the ratio

$$R_{d_1} = \frac{C_{3\,\mathrm{pt}}^{\Gamma,\mathcal{O}_{[34]}^{5q}}}{C_{2\,\mathrm{pt}}} = d_1. \tag{24}$$

IV. RENORMALIZATION

The local operators discussed in the previous section arise from an operator product expansion and therefore must be renormalized. The renormalized operators defined at scale μ are obtained from lattice-regularized operators defined with lattice spacing a.

$$\mathcal{O}_i(\mu) = Z_i(\mu, a)\mathcal{O}_i(a) + \sum_{j\neq i} a^{d_j-d_i}Z_{ij}(\mu, a)\mathcal{O}_j(a), \tag{25}$$

where $\mathcal{O}_j$ are a set of operators allowed by symmetries to mix among themselves, and d_j is the dimension of each operator. If mixing with lower dimensional operators occurs, the mixing coefficients are power divergent, and hence must be computed nonperturbatively to accurately subtract them. The mixing of lattice operators is more complicated than that of the continuum operators since not all of the continuum symmetries are respected on the lattice. In particular, $O(4)$ rotational symmetry in Euclidean space is broken down to the hypercubic group H(4). As a result, an irreducible representation of $O(4)$ is reducible under H(4) and hence mixing of operators that would not occur in the continuum can occur on the lattice. For a detailed analysis of the H(4) group representations see [32,39] and references therein. The lattice operators are selected carefully so mixing with lower dimensional operators does not occur and thus no power divergences are encountered. In general, the breaking of rotational symmetry makes the calculation of higher spin operators (and thus higher moments of structure functions) difficult.

The breaking of chiral symmetry (e.g., by the lattice) results in mixings with lower dimensional operators for the d_n matrix elements. The problem is avoided by using chiral lattice fermions such as domain wall, overlap, or fixed point fermions.

In order to renormalize the quark bilinear operators studied here, we employ the nonperturbative renormalization (NPR) method introduced in [40]. This method has been shown to work very well in the case of domain wall fermions [41,42]. For quark bilinears without derivatives we only need to compute a single quark propagator from a point source; the Fourier transform then yields the quark propagator $\mathbf{S}(pa;0)$ in momentum space which is sufficient to calculated all of the needed vertices.

$$\mathbf{S}(pa;0) = \sum_x e^{-ip\cdot x}\mathbf{S}(x;0), \tag{26}$$

where the lattice momentum p_μ is

$$p_\mu = \frac{2\pi}{L_\mu}n_\mu \qquad (n_\mu = 0, \pm 1, \pm 2, \ldots), \tag{27}$$

where L_μ is the linear lattice size in direction μ. Because the NPR method relies on matrix elements of the operators between off-shell quark and gluon states, the calculation proceeds in a fixed gauge which, for convenience, is chosen to be the Landau gauge.

In the case of operators containing derivatives, a single quark propagator is not sufficient to build the quark bilinears we need. One way to proceed is the method in [43] where propagators with momentum sources instead of point sources are prepared in Landau gauge and derivative

(difference) operators are constructed at the sink point where values at all neighboring points are available. This method works well when operators with many derivatives are needed but is expensive if many values of momentum are desired.

In our case we are only interested in operators with one derivative which can be constructed from a point-source propagator and a point-split-source propagator with appropriate gauge links attached at the source.

$$\mathbf{S}_\mu(pa;0) = \sum_x e^{-ip\cdot x}\frac{1}{2}[\mathbf{S}(x;-\hat{\mu})U_\mu(-\hat{\mu}) - \mathbf{S}(x;\hat{\mu})U_\mu^\dagger(0)]. \quad (28)$$

Following this strategy, we compute the matrix elements of derivative operators with many values of momentum by computing four additional quark propagators on each gauge configuration.

Following [41], we define the amputated, bare, vertex function for each operator $\mathcal{O}$,

$$\mathcal{V}^{\mathcal{O}}(p^2) = \frac{1}{\langle S^\dagger(p)\rangle}\langle S^\dagger(p)\mathcal{O}S(p)\rangle\frac{1}{\langle S(p)\rangle} \quad (29)$$

and a corresponding projector that enforces the tree-level renormalization condition

$$\mathrm{Tr}\,\mathcal{P}\mathcal{V}^{\mathcal{O}} \propto 1. \quad (30)$$

We choose the following,

$$\mathcal{O}^{q}_{\{44\}} \to \mathcal{P}^{q-1}_{44} = \gamma_4 p_4 - \frac{1}{3}\sum_{i=1,3}\gamma_i p_i, \quad (31)$$

$$\mathcal{O}^{5q}_{\{34\}} \to \mathcal{P}^{5q-1}_{34} = i\gamma_5\frac{1}{2}[\gamma_3 p_4 + \gamma_4 p_3], \quad (32)$$

$$\mathcal{O}^{\sigma q}_{34} \to \mathcal{P}^{\sigma q-1}_{34} = \gamma_5\sigma_{34}. \quad (33)$$

Defining the renormalized operator at scale $\mu^2 = p^2$ as $\mathcal{O}_{\mathrm{ren}}(\mu) = Z_{\mathcal{O}}(\mu, a)\mathcal{O}(a)$, the renormalized vertex takes the form

$$\mathcal{V}^{\mathcal{O}}_{\mathrm{ren}}(p^2) = \frac{Z_{\mathcal{O}}}{Z_q}\mathcal{V}^{\mathcal{O}}(p^2), \quad (34)$$

and after projection,

$$\Lambda_{\mathcal{O}_{\mathrm{ren}}}(p^2) = \frac{Z_{\mathcal{O}}}{Z_q}\Lambda_{\mathcal{O}}(p^2) = \frac{1}{\mathrm{Tr}\mathcal{P}^2_{\mathcal{O}}(p)}\,\mathrm{Tr}[\mathcal{P}_{\mathcal{O}}(p)\mathcal{V}^{\mathcal{O}}(p^2)]\frac{Z_{\mathcal{O}}}{Z_q}. \quad (35)$$

From this we extract the required renormalization constant $Z_{\mathcal{O}}$ that ensures the same renormalization condition at scale μ as in the free case.

$$\Lambda_{\mathcal{O}_{\mathrm{ren}}}(\mu^2) = \frac{Z_{\mathcal{O}}}{Z_q}\Lambda_{\mathcal{O}}(\mu^2) = 1. \quad (36)$$

A. Anomalous dimensions and matching

In order to compute the renormalization group invariant (RGI) constants [40], we divide out the running of the operator at hand, calculated in continuum perturbation theory. To be sensible, this is done at large enough momentum so the operator runs perturbatively. The momentum cannot be taken too large, or lattice artifacts will spoil the continuum running of the operator. Thus the momentum scale where the RGI constant is defined must satisfy

$$\Lambda_{\mathrm{QCD}} \ll \mu \ll \frac{1}{a}. \quad (37)$$

In addition, it is convenient to match the RI/MOM regularization used in NPR with the $\overline{MS}$ scheme since the latter is conventionally used in the Wilson coefficient calculation. For the derivative operators the matching from the RI/MOM scheme in Landau gauge to $\overline{MS}$ can be done using the conversion factor [43]

$$Z^{\overline{MS}}_{\mathrm{MOM}}(p) = 1 + \frac{\alpha_s}{4\pi}C_F\Big[G_n + S_{n-1} - \frac{2(n-1)}{n(n+1)} \times \frac{(\sum_\mu p_\mu h_\mu(p))^2}{p^2\sum_\mu h_\mu(p)^2}\Big] + O(\alpha_s^2), \quad (38)$$

where $C_F = \frac{N_c^2-1}{2N_c}$ is the quadratic Casimir for the $SU(N_c)$ gauge group, α_s the strong coupling constant,

$$G_n = \frac{2}{n(n+1)}(2S_{n+1} - 3 - S_{n-1}) + \frac{2}{n+1} - 4\sum_{j=2}^{n}\frac{1}{j}(2S_j - S_{j-1}) - 1, \quad (39)$$

$$S_n = \sum_{j=1}^{n}\frac{1}{j}, \quad (40)$$

and

$$h_\mu(p) = \sum_{\mu_2,\ldots,\mu_n} c_{\mu\mu_2\ldots\mu_n}p_{\mu_2}\cdots p_{\mu_n}. \quad (41)$$

The conversion factor $Z^{\overline{MS}}_{\mathrm{MOM}}$ depends on the direction of the momentum p and on the coefficients $c_{\mu_1,\ldots,\mu_n}$ because the renormalization condition breaks $O(4)$ invariance. The coefficients $c_{\mu_1,\ldots,\mu_n}$ are defined using the conventions in [43]. In the present case for the momentum fraction and helicity operators we have

$$c_{\mu\nu} = \delta_{\mu 4}\delta_{\nu 4} - \frac{1}{3}\sum_{k=1}^{3}\delta_{\mu k}\delta_{\nu k}, \quad (42)$$

and

$$c_{\mu\nu} = \delta_{\mu 3}\delta_{\nu 4} + \delta_{\mu 4}\delta_{\nu 3}, \quad (43)$$

respectively.

For matching the tensor bilinear we use results from [44].

$$Z_{\mathrm{MOM}}^{\overline{MS}} = 1 - \left(\frac{\alpha_s}{4\pi}\right)^2 \frac{C_F}{216}[(4320\zeta(3) - 4815)C_F - 1252T_F n_f + (5987 - 3024\zeta(3))C_A] + O(\alpha_s^3) \tag{44}$$

where $\zeta(k)$ is the Riemann zeta function, $C_A = N_c$ and $T_F = 1/2$ for the $SU(N_c)$ group.

In our analysis, we first match $\Lambda_{\mathcal{O}}$ to $\overline{MS}$ and then use the $\overline{MS}$ running of the operators to extract the RGI renormalization constant.

Following the conventions of [41], the continuum two-loop running of the operators is parametrized by

$$C_{\mathcal{O}}(\mu^2) = \alpha_s(\mu)^{\bar{\gamma}_0}\left\{1 + \frac{\alpha_s(\mu)}{4\pi}(\bar{\gamma}_1 - \bar{\beta}_1\bar{\gamma}_0)\right\}, \tag{45}$$

where the anomalous dimension of the operator is

$$\gamma_{\mathcal{O}} = \sum_i \gamma_{\mathcal{O}}^{(i)}\left(\frac{\alpha_s}{4\pi}\right)^{i+1} \tag{46}$$

$$\bar{\gamma}_{\mathcal{O}i} = \frac{\gamma_{\mathcal{O}}^{(i)}}{2\beta_0} \tag{47}$$

$$\bar{\beta}_i = \frac{\beta_i}{\beta_0}, \tag{48}$$

and $\beta_{0,1}$ are the first two coefficients in the weak coupling expansion of the beta function

$$\frac{\beta(\alpha_s)}{4\pi} = -\beta_0\left[\frac{\alpha_s}{4\pi}\right]^2 - \beta_1\left[\frac{\alpha_s}{4\pi}\right]^3 - \ldots. \tag{49}$$

The two-loop running of α_s is given by [45,46]

$$\frac{\alpha_s}{4\pi} = \frac{1}{\beta_0 \ln(\mu^2/\Lambda_{\mathrm{QCD}}^2)} - \frac{\beta_1 \ln\ln(\mu^2/\Lambda_{\mathrm{QCD}}^2)}{\beta_0^3 \ln^2(\mu^2/\Lambda_{\mathrm{QCD}}^2)} \tag{50}$$

TABLE I. The one- and two-loop expansion coefficients of the quenched QCD β function.

β_i	quenched ($n_f = 0$) value
β_0	11
β_1	102

TABLE II. Anomalous dimensions of quark bilinear operators used in this paper in quenched ($n_f = 0$) QCD.

Operator	γ_0	γ_1
$\mathcal{O}_{44}^{q}$	64/9	96.69
$\mathcal{O}_{\{34\}}^{5q}$	64/9	96.69
$\mathcal{O}_{34}^{\sigma q}$	8/3	724/9

The values of the β_i's and the γ_i's used in this analysis are given in Tables I and II respectively. For Λ_{QCD} we take the quenched value [47], $\Lambda_{\mathrm{QCD}} = 238 \pm 19$ MeV.

V. NUMERICAL DETAILS

We work in the quenched approximation and use domain wall fermions to compute the matrix elements described in the previous sections. We use the DBW2 gauge action [48,49] at lattice spacing $a^{-1} \approx 1.3$ GeV ($\beta = 0.87$), with lattice size $16^3 \times 32$ and fifth dimension $L_s = 16$. This action has been shown to significantly reduce the explicit chiral symmetry breaking of domain wall fermions with finite fifth dimension relative to the Wilson gauge action [31]. This relatively coarse lattice spacing was chosen to give a large physical volume (2.4 fm spatial size) and enable calculations with light quark masses to study the chiral behavior of the matrix elements. An earlier calculation of the nucleon axial charge showed that such a large volume is necessary to avoid significant finite volume errors [21] which, based on that study, we may expect to be a few percent for pion masses in the range 390 MeV–850 MeV. The residual quark mass for $L_s = 16$ at this lattice spacing and for the DBW2 action is $m_{\mathrm{res}} \approx 0.7$ MeV [31], truly negligible compared to the input quark masses in our simulation, $0.02 \leq m_f \leq 0.1$, which span a range from about one-quarter to 2 times the strange quark mass [31].

To calculate three point correlation functions we use box sources with size $\sim$1.2 fm and sequential-source propagators with point sinks. For details see [21]. The source time

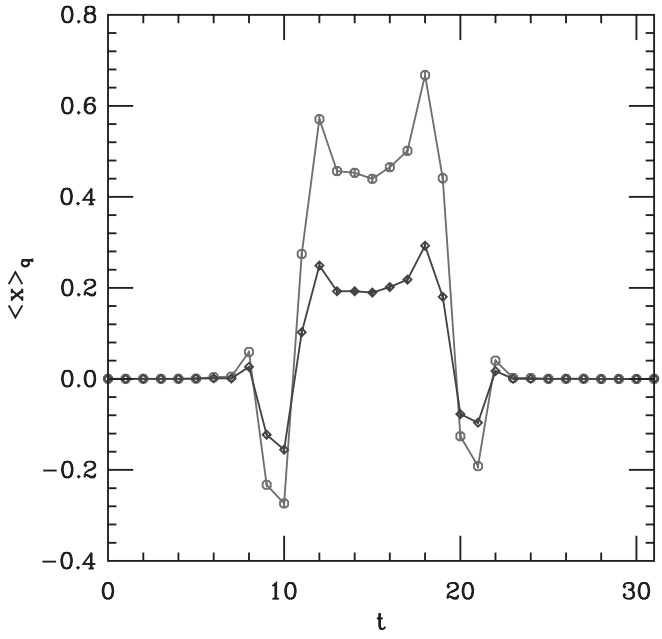

FIG. 1. The three point correlation function for the operator $\mathcal{O}_{44}^{q}$ and bare quark mass $m_f = 0.04$. Octagons are the up quark contribution and diamonds are the down quark contribution.

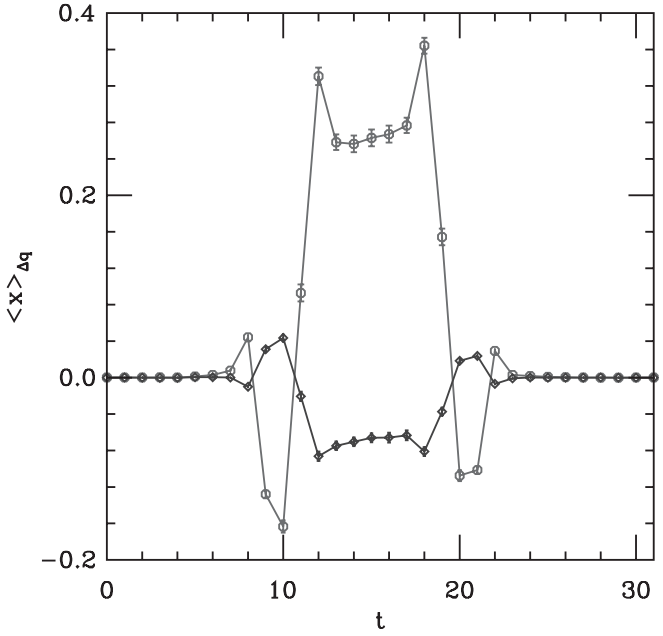

FIG. 2. The three point correlation function for the operator $\mathcal{O}^{5q}_{\{34\}}$ and bare quark mass 0.04. Octagons are the up quark contribution and diamonds are the down quark contribution.

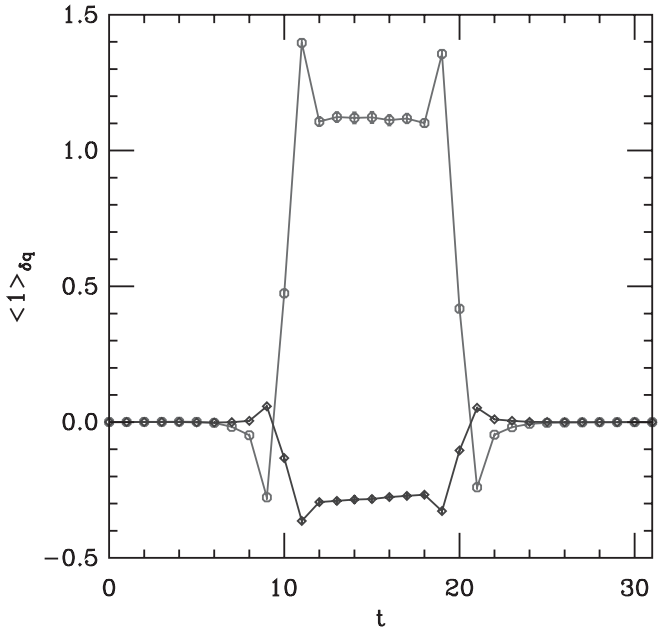

FIG. 4. The three point correlation function for the operator $\mathcal{O}^{\sigma q}_{34}$ and bare quark mass 0.04. Octagons are the up quark contribution and diamonds are the down quark contribution.

is $t = 10$ and the source-sink time separation is 10 lattice units, approximately 1.5 fm, which provides a sufficiently large time separation to observe clear plateaus. Figures 1–4 show typical plateaus for the matrix elements studied in this work. Our calculation is done using 416 independent gauge configurations produced using the overelaxed heat-bath algorithm described in [31]. All statistical errors are jackknife estimates.

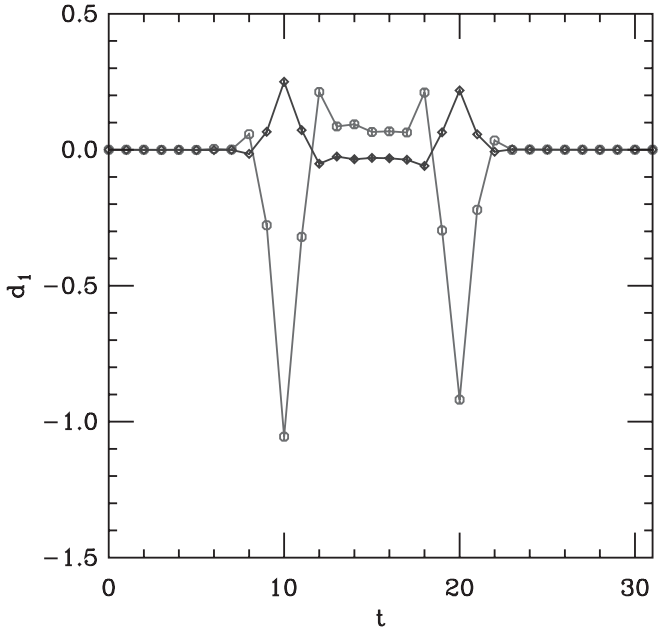

FIG. 3. The three point correlation function for the operator $\mathcal{O}^{5q}_{[34]}$ and bare quark mass 0.040. Octagons are the up quark contribution and diamonds are the down quark contribution.

For the calculation of renormalization constants we use 120 lattices and fix to Landau gauge using the technique described in [41]. Two-loop continuum running is used to extract the RGI renormalization constants in all cases. In order to eliminate remaining scaling violations we fit the data linearly in $(ap)^2$ and define the renormalization constant from the intercept (as done in [41]). The fitting range used is $(pa)^2 \in [1.2, 1.9]$.

VI. RESULTS AND DISCUSSION

The nucleon mass has been determined on a subset of this ensemble of lattices previously [31]. For the present analysis, we fit the two-point correlation function to a single exponential from time $t = 6$ to 15. The fitted nucleon mass for each quark mass is given in Table III; they are consistent with those reported in [31].

The central question we sought to answer with this study is why lattice results for the first moments of the polarized and unpolarized structure functions disagree with fits to experimental measurements [13,15,25,26,50,51]. Preliminary results from this study and one using two flavors of dynamical domain wall fermions have been reported in [17,19,20]. The discrepancy is large ($\gtrsim$ 50%), and holds for dynamical as well as quenched calculations. A plausible explanation is that the quarks simulated in these past studies, valence and sea, have been too heavy. Here we use as light a quark mass that has been simulated to date for nucleon structure calculations,

TABLE III. The nucleon mass in lattice units. Values are from fully covariant, single exponential, fits to the two-point correlation functions in the range $6 \leq t \leq 15$. Errors are statistical only.

m_f	m_N (error)	χ^2 (dof)
0.02	0.856(10)	5.9(8)
0.04	0.967(6)	1.9(8)
0.06	1.064(5)	3.5(8)
0.08	1.155(4)	5.1(8)
0.10	1.241(4)	6.4(8)

roughly one-quarter of the strange quark mass, in order to investigate the chiral regime. If the problem is related to the sea quark mass, a resolution will have to wait for future dynamical fermion calculations using lighter sea quark masses than have been used already.[2]

In Fig. 5 and Table IV we present our results for the momentum fraction, $\langle x \rangle_q$, of the up and down valence quarks. These results do not contain disconnected diagrams. Figure 6 shows the isovector matrix element $\langle x \rangle_{u-d}$ where disconnected diagrams do not contribute (for degenerate u, d quarks). The central values are obtained from a constant fit over the range $13 \leq t \leq 16$, based on the plateau in Fig. 1 (the same range is used for all matrix elements in this work). The quark mass dependence is mild and appears linear. The renormalization constant corresponding to the momentum fraction is $Z^{\overline{MS}}(2\ \text{GeV}) = 1.02(10)$, essentially one, (see Fig. 13 and Table VII). The renormalized results are all significantly higher than the value 0.154(3) extracted from the experimental data of [7,10,12] by Dolgov *et al.* [15], and the more recent value of 0.180(5) extracted by the parameterization of [52]. In addition, there is no apparent curvature as $m_\pi^2 \rightarrow 0$ that leads us to believe that in the chiral limit the two results would agree. Thus, we do not attempt to extrapolate to $m_\pi^2 = 0$. This is the same behavior witnessed in previous studies; in particular, our $\overline{MS}$ values for $\langle x \rangle_q$ are quite consistent with the recently reported quenched improved Wilson fermion, continuum and chiral limit, value in [25], suggesting good scaling of domain wall fermions. Finally, we should mention that a recent overlap calculation finds a smaller value than ours, but is result is unrenormalized [53].

Figure 7 shows the first moment of the helicity distribution $\langle x \rangle_{\Delta q}$ for the up and down quarks (tabulated in Table V). As before, these results do not contain disconnected diagrams, and in Fig. 8 we display the isovector matrix element $\langle x \rangle_{\Delta u - \Delta d}$ where disconnected diagrams do not contribute. Again, the quark mass dependence is mild

[2]The RBC and UKQCD collaborations are embarking on a large scale project this year to generate an extensive ensemble of $2 + 1$ flavor domain wall fermion lattices with sea quark masses as light as $1/5$ the strange quark mass. Among many other quantities, nucleon structure will be studied

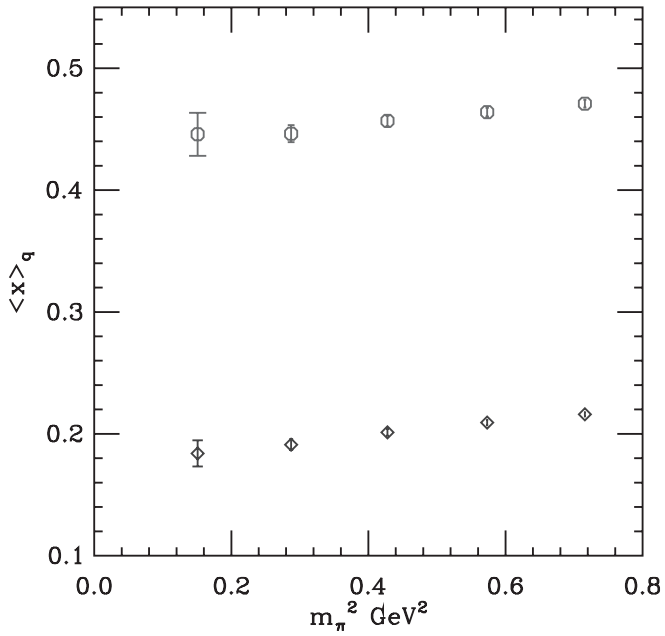

FIG. 5. The bare momentum fraction. m_π is the pseudoscalar mass. Octagons are the up quark contributions and diamonds are the down quark contributions. Disconnected diagrams are not included.

TABLE IV. Lowest moment of unpolarized structure functions for u and d quarks and the flavor nonsinglet combination. Errors are statistical only. Values are not renormalized.

m_f	$\langle x \rangle_u$	$\langle x \rangle_d$	$\langle x \rangle_{u-d}$
0.020	0.446(18)	0.184(11)	0.262(16)
0.040	0.446(7)	0.191(4)	0.255(6)
0.060	0.457(5)	0.2012(28)	0.256(3)
0.080	0.464(4)	0.2092(21)	0.2548(25)
0.100	0.471(3)	0.2160(18)	0.2549(21)

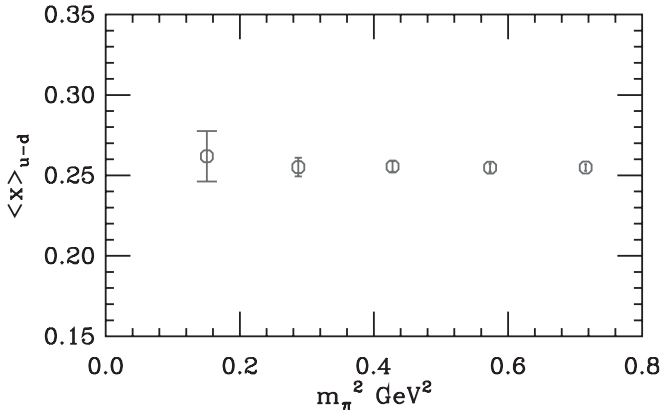

FIG. 6. The bare flavor nonsinglet momentum fraction.

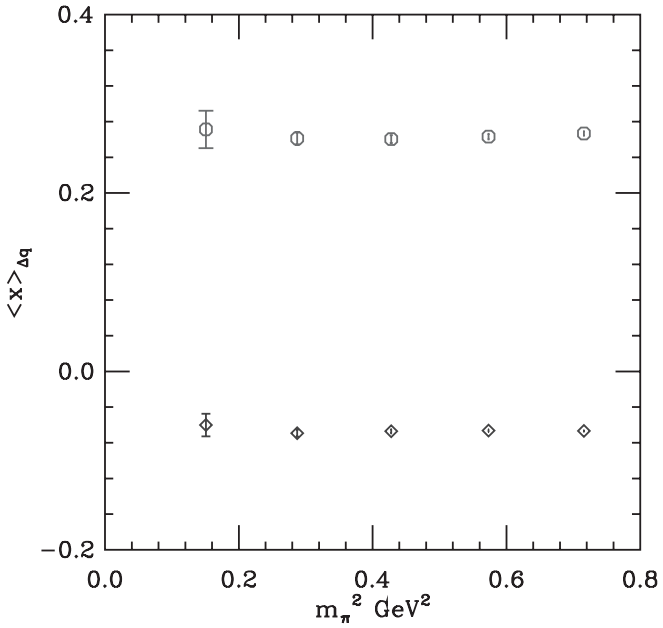

FIG. 7. The bare helicity distribution. Octagons are the up quark contributions and diamonds are the down quark contributions. Disconnected diagrams are not included.

and appears linear, the renormalization constant is essentially unity, $Z^{\overline{MS}}(2\ \mathrm{GeV}) = 1.02(9)$ (see Fig. 14 and Table VII), and the renormalized moments lie above the value 0.196(4) extracted from the experimental data of [5,6] by Dolgov *et al.* [15].

Since chiral symmetry requires that the renormalization constants of the momentum fraction and the helicity distribution be the same, we can consider the ratio of the bare matrix elements in which the renormalization constants and matching factors cancel. A similar ratio worked well in the case of the axial charge, g_A [21], and we saw already that the explicit calculations of these constants gave the same result well within statistical errors. Figure 9 shows the ratio together with the value extracted from experiment [5–12,15]. As it is argued in [15], it is difficult to estimate the systematic errors associated with the experimental extraction of the values of both $\langle x\rangle_{u-d}$ and $\langle x\rangle_{\Delta u-\Delta d}$ but it is almost certain that these systematic errors are smaller

TABLE V. Lowest moment of the polarized structure fucntions. Errors are statistical only. u and d valence quark contributions. $\Delta u - \Delta d$ denotes the flavor nonsinglet combination. Errors are statistical only. Values are not renormalized.

m_f	$\langle x\rangle_{\Delta u}$	$\langle x\rangle_{\Delta d}$	$\langle x\rangle_{\Delta u-\Delta d}$
0.020	0.271(21)	−0.060(13)	0.331(23)
0.040	0.261(7)	−0.069(4)	0.330(8)
0.060	0.260(4)	−0.0671(23)	0.328(5)
0.080	0.263(3)	−0.0664(16)	0.330(4)
0.100	0.2667(26)	−0.0667(12)	0.3335(29)

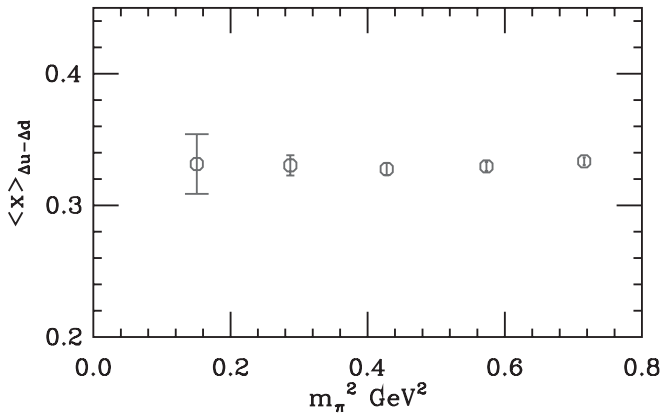

FIG. 8. The bare flavor nonsinglet helicity distribution.

than the statistical errors of the lattice calculation. For that reason the comparison of lattice results to experiment is not out of order. Interestingly, our results are in very good agreement with experiment; a discrepancy is not evident at all. Note that the jackknife determination of the ratio is determined relatively precisely since the error on the renormalization constants does not enter and the numerator and denominator are highly correlated.

In [21] the axial and vector matrix elements displayed very different finite volume behavior as the quark mass was reduced; the axial matrix element, being sensitive to low energy physics, decreased drastically in the limit $m_f \rightarrow 0$ in the small volume study. If similar behavior is operative here, the mild quark mass dependence of the matrix elements suggests that finite volume effects are small.

In [51] the quark mass dependence near the chiral limit of $\langle x\rangle_{u-d}$ but not of $\langle x\rangle_{\Delta u-\Delta d}$, was computed in quenched chiral perturbation theory, so we can not say what the chiral perturbation theory prediction is for the ratio. For $\langle x\rangle_{u-d}$

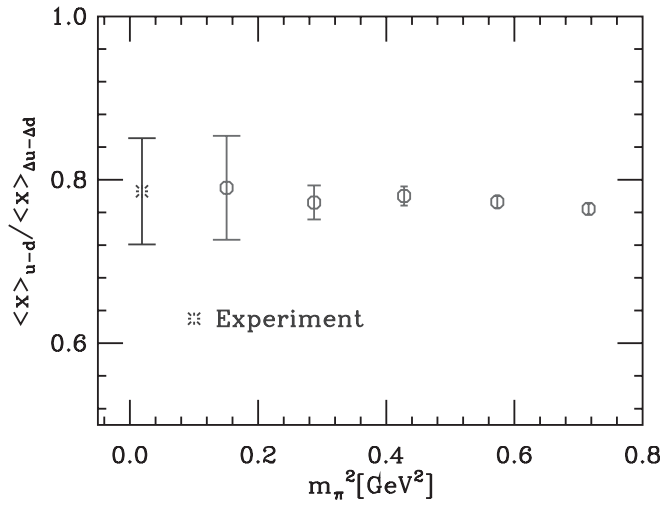

FIG. 9. The ratio of the flavor nonsinglet momentum fraction to the helicity distribution (octagons). The experimental expectation is marked by the burst symbol.

alone, the chiral perturbation theory formula allows a wide range of values at the physical point, depending on the values of various unknown low energy constants. The authors of [51] investigate the quark mass dependence for several values of the unknown parameters. The most natural choice demonstrates a smaller dependence on the quark mass than that predicted by full QCD chiral perturbation theory.

Our results suggest that whatever systematic error causes the discrepancy in the individual moments from experimental expectations appears to mostly cancel in their ratio. Although our calculation is quenched, it is instructive to look at the full QCD chiral perturbation theory formulas found in [50,54].

$$\langle x\rangle_{u-d} = C\left[1 - \frac{3g_A^2+1}{(4\pi f_\pi)^2} m_\pi^2 \ln\left(\frac{m_\pi^2}{\mu^2}\right) + e(\mu^2)\frac{m_\pi^2}{(4\pi f_\pi)^2}\right] \tag{51}$$

$$\langle x\rangle_{\Delta u-\Delta d} = \tilde{C}\left[1 - \frac{2g_A^2+1}{(4\pi f_\pi)^2} m_\pi^2 \ln\left(\frac{m_\pi^2}{\mu^2}\right) + \tilde{e}(\mu^2)\frac{m_\pi^2}{(4\pi f_\pi)^2}\right] \tag{52}$$

where the normalization is such that the physical pion decay constant is $f_\pi = 93$ MeV, C and $\tilde{C}$ are unknown constants, and $e(\mu^2)$ and $\tilde{e}(\mu^2)$ are counter terms evaluated at the renormalization scale μ. In Fig. 16 we plot the above formulas for $\mu = 1$ GeV. The unknown constants C and $\tilde{C}$ are chosen so that the formulae reproduce the experimental result at the physical pion mass point, and the counter terms are set to zero in order to isolate the effect of the chiral logarithm. We see that there is a strong dependence on the pion mass. As a result, when $m_\pi \approx 400$ MeV, the momentum fraction is roughly 50% larger than at the physical point, while the first moment of the helicity is about 30% larger. This indicates that the discrepancy between the lattice data and experiment may be due to the unphysically large masses used in current lattice simulations. On the other hand, the large size of the one-loop perturbative corrections suggests that chiral perturbation theory at this order is unreliable. The effects of the counter terms and higher order contributions may also be large and could tend to cancel the large one-loop corrections. Nevertheless, it is worth noting that our quenched results at pion masses of about 400 MeV differ from experiment by roughly the same amount as one-loop chiral perturbation theory in full QCD predicts. The observation of the large one-loop corrections was first made by the authors of [26,55–57].

On the other hand the ratio of the momentum fraction to the first moment of the helicity (Fig. 17) is a milder function of the quark mass. The difference of the experimental result from the value at $m_\pi = 400$ MeV is about 10%, not wildly inconsistent with the lattice result shown in Fig. 9.

TABLE VI. The twist-3 matrix element d_1. u and d valence quark contributions. Errors are statistical only. Values are not renormalized.

m_f	d_{1u}	d_{1d}
0.020	0.045(21)	−0.029(14)
0.040	0.075(8)	−0.031(5)
0.060	0.109(5)	−0.0354(29)
0.080	0.140(4)	−0.0405(20)
0.100	0.167(3)	−0.0457(15)

The conclusion from this discussion is that the discrepancy between lattice and experimental results for the quark momentum fraction and helicity distribution is most likely due to strong mass dependence in these functions and will be resolved by pushing lattice simulations further into the light quark mass region. Since dynamical results so far are similar to quenched [19,20], this probably holds in that case too. It may also be of interest to obtain the next higher order results in chiral perturbation theory for these quantities, though this seems a more daunting task.

We now turn to another interesting feature in our calculation, the twist-3 matrix element d_1. Although it is not measurable in deep inelastic scattering of electrons on protons, it serves as an example of what can be expected for the d_n matrix elements. As discussed in Sec. IV, the operator used to calculate d_1, $\mathcal{O}^{5q}_{[\mu\nu]}$, mixes with the lower dimensional operator $\mathcal{O}^{\sigma q}_{\mu\nu}$ when chiral symmetry is explic-

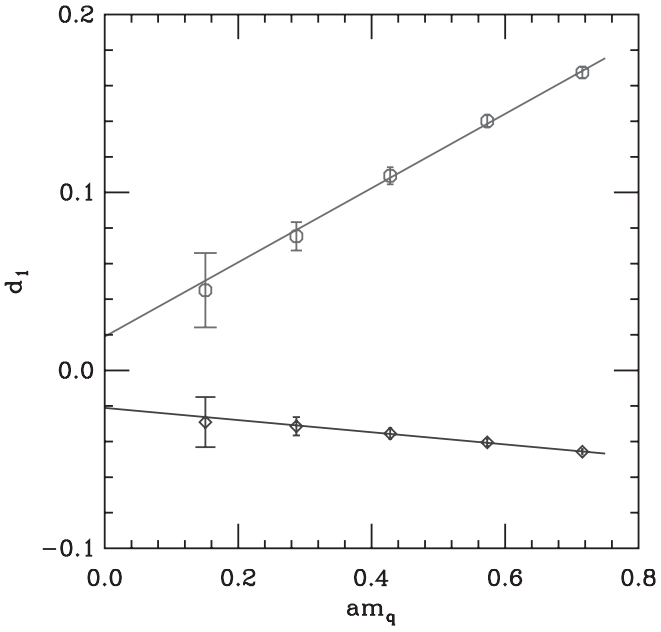

FIG. 10. The bare d_1. Octagons are the up quark contributions and diamonds are the down quark contributions. Disconnected diagrams are not included.

itly broken. With domain wall fermions, unlike Wilson fermions, chiral symmetry is not broken ($m_{\rm res}$ is small enough to ignore in this study), so power divergent mixing should not occur. Results are summarized in Table VI. Figure 10 shows, unlike the Wilson fermion result [15], this matrix element is small in the chiral limit. In fact, the power divergence in the Wilson fermion case switches the sign of the u and d quark contributions. Using Wilson fermions, the QCDSF collaboration found similar results for d_2 after a nonperturbative subtraction of the power divergence [38]. These results confirm our expectations that the domain wall fermion formulation avoids the power divergence present for Wilson fermions. Because the value of d_1 computed here and QCDSF's value of d_2 appear small in the chiral limit, we conclude that the Wandzura-Wilczek relation between moments of g_1 and g_2 [58], which assumes vanishing d_n, is at least approximately true. This relation is not obvious in a confining theory [59].

Finally, we have computed the first moment of the transversity distribution, $\langle 1\rangle_{\delta q}$, for up and down quarks (Fig. 11) and the isovector combination $\langle 1\rangle_{\delta u-\delta d}$ (Fig. 12). The transversity is an important target of the RHIC spin program at Brookhaven National Laboratory (see [60,61] and references therein). In both cases the quark mass dependence is mild and appears to be linear. The renormalization constant (Fig. 15 and Table VII) is $Z^{\overline{MS}}(2\ \text{GeV}) = 0.872(11)$. Naive linear extrapolation to the chiral limit yields $\langle 1\rangle_{\delta u-\delta d} = 1.193(30)$ for $\mu = 2$ GeV in the $\overline{MS}$ scheme. This result contains an unknown systematic error from the chiral extrapolation which may be small given the mass dependence exhibited in Fig. 12. We note that the calculation of the flavor nonsinglet tensor charge is similar to g_A which also exhibited mild mass dependence and whose value agrees well with experiment [21]. We caution the reader that the momentum fraction and helicity distribution also exhibited mild mass dependence but are known to disagree with fits to the experimental data. Our value is consistent with another recent calculation [62].

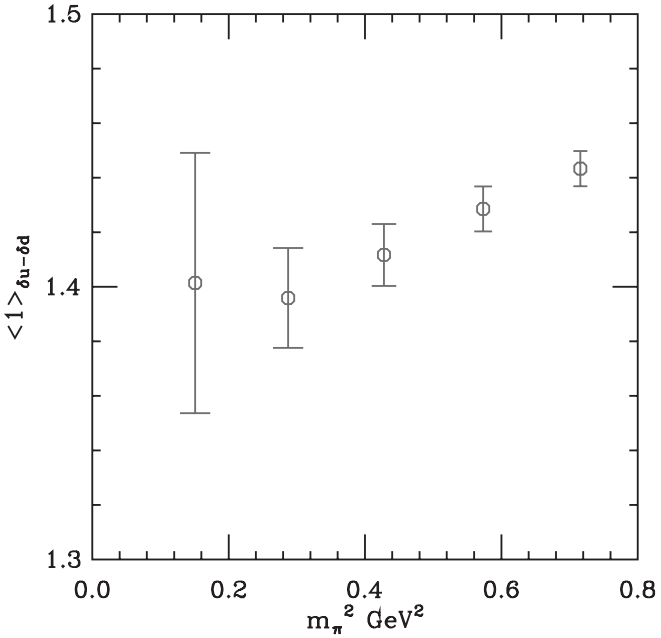

FIG. 12. The bare flavor nonsinglet transversity.

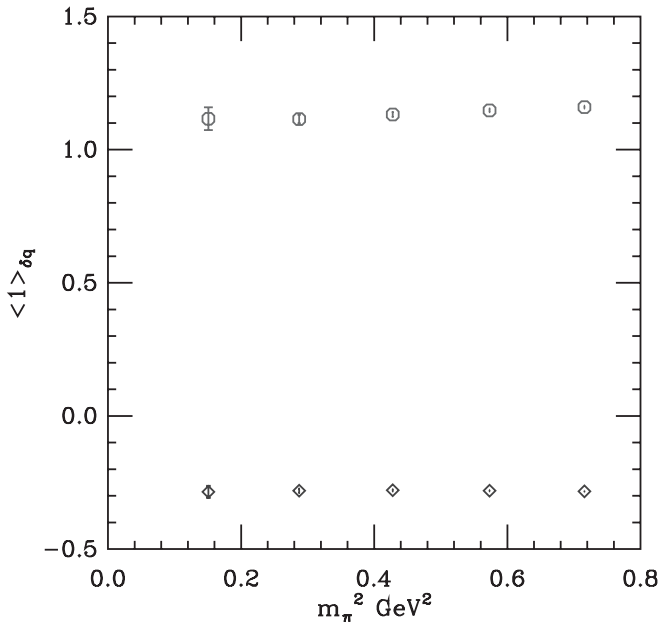

FIG. 11. The bare transversity. Octagons are the up quark contributions and diamonds are the down quark contributions. Disconnected diagrams are not included.

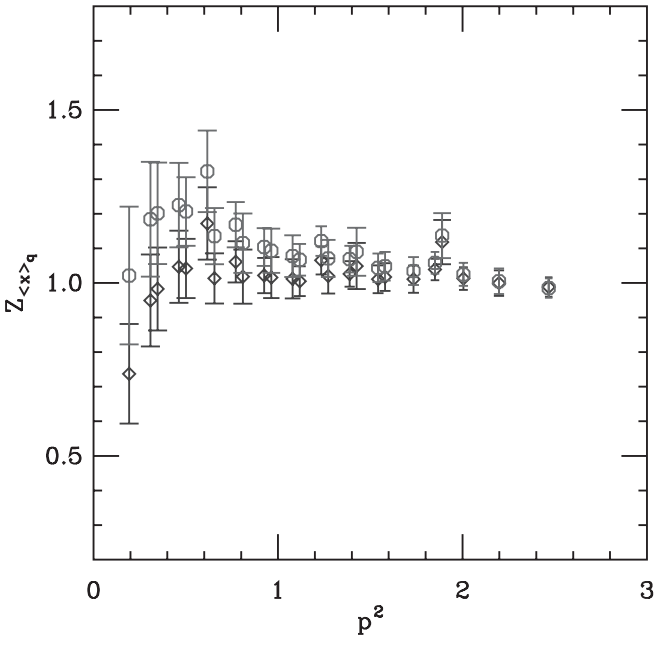

FIG. 13. Renormalization constant for the momentum fraction. The diamonds are the renormalization group invariant points. The octagons are the raw data.

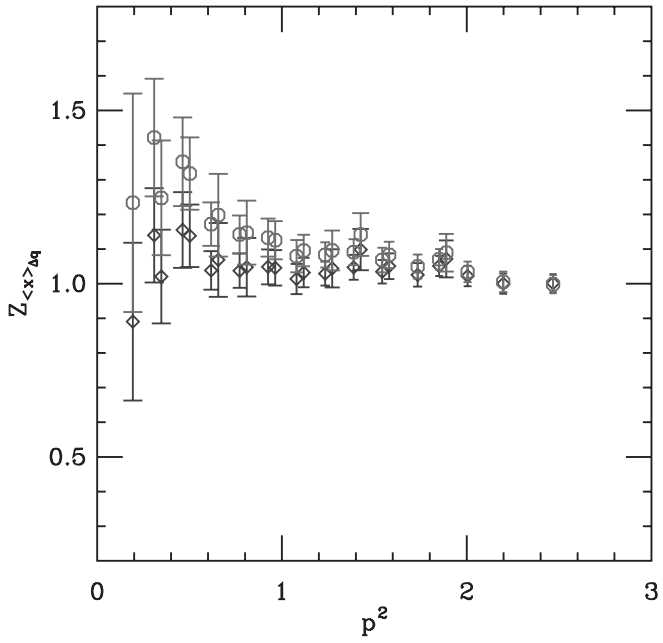

FIG. 14. Renormalization constant for the helicity distribution. The diamonds are the renormalization group invariant points. The octagons are the raw data.

VII. CONCLUSIONS

We have reported on a quenched calculation of the first moments of the polarized and unpolarized structure functions of the nucleon. We have used domain wall fermions in a relatively large physical volume, $\sim(2.4\ \mathrm{fm})^3$. The large volume is important to minimize finite volume errors in nucleon matrix element calculations as shown earlier in the calculation of the axial charge, g_A [21]. The chiral symmetry of domain wall fermions may also be useful in unraveling the mystery of the large discrepancy between lattice calculations and experiment for the moments of structure functions. While our results for the individual moments show no evidence of the chiral logarithm predicted in [50,51,54,63] for pion masses as low as 390 MeV, the ratio of the momentum fraction to the first moment of the helicity distribution is in very good agreement with the experimental value (Fig. 9). We note that the ratio is computed on the lattice more accurately than the individual moments. This agreement, taken together with chiral perturbation theory calculations, leads us to conclude that the discrepancy between lattice calculations and fits to experiment is most likely due to strong mass dependence of these functions in the light quark regime. Thus, ultimately the difference will be resolved as lattice calculations push into this regime.

A recent large scale, detailed, investigation of the discrepancy in low moments of nucleon structure functions was reported in [25]; using improved Wilson fermions, the authors performed continuum and chiral extrapolations but did not resolve the problem. The agreement with our results suggests that scaling violations for domain wall fermions are mild (the coarsest lattice spacing used in [25] was about 0.1 fm compared to 0.15 fm used here).

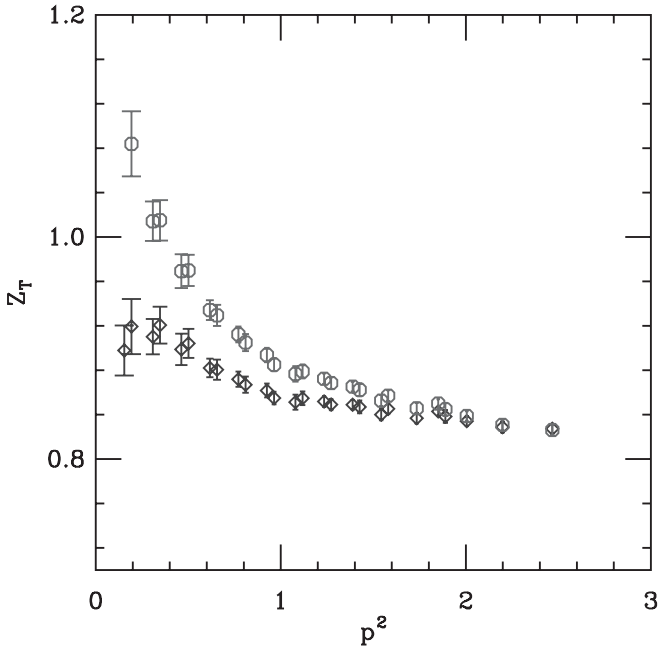

FIG. 15. Renormalization constant for the transversity. The diamonds are the renormalization group invariant points. The octagons are the raw data.

TABLE VII. The $\overline{MS}$ renormalization constants at $\mu = 2$ GeV. Errors are statistical only.

$Z_{\langle x\rangle_q}$	1.02(9)
$Z_{\langle x\rangle_{\Delta q}}$	1.02(10)
Z_T	0.872(11)

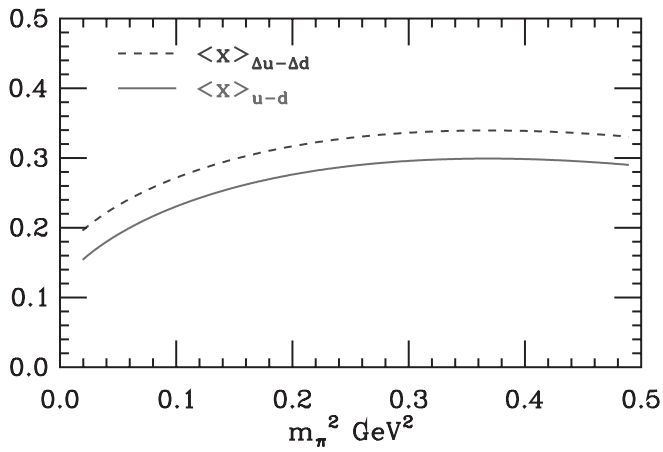

FIG. 16. The leading chiral logarithm dependence for the first moment of the helicity and the momentum fraction. The curves are normalized so that at the physical point the experimental result is recovered.

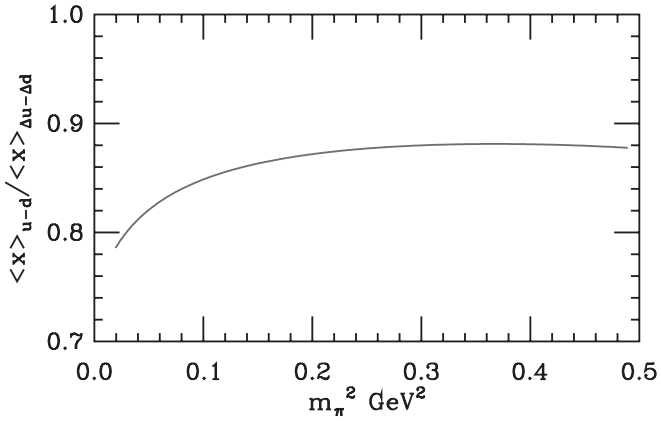

FIG. 17. The leading chiral logarithm dependence for the ratio of the momentum fraction to the first moment of the helicity. The curve is normalized so that at the physical point the experimental result is recovered.

Our calculation of the d_1 matrix element (Fig. 10) indicates that the domain wall formalism eliminates power divergent mixing in this class of matrix elements. This suggests that a precision calculation of d_2 with domain wall (or other chiral) fermions is possible and should be undertaken. Since the mixing with lower dimensional operators induced by explicit chiral symmetry breaking is linearly divergent with a^{-1}, care must be taken to minimize m_{res}.

Finally, we have computed the first moment of the transversity distribution, or tensor charge, which will be measured at Brookhaven National Laboratory as part of the RHIC spin program. We find $\langle 1 \rangle_{\delta u - \delta d} = 1.193(30)$ at $\mu = 2$ GeV in the $\overline{MS}$ scheme, with unknown systematic error stemming from the linear chiral extrapolation. The mild quark mass dependence in the tensor charge suggests this systematic error is small, as does the similarity to the calculation of g_A. On the other hand, such mild mass dependence is also observed in the momentum fraction and helicity distribution, hence further study of the chiral extrapolation of this observable is needed in order to obtain a reliable estimate of the systematic error.

An unknown systematic error due to quenching exists in our results. Two flavor calculations using Wilson fermions with relatively heavy quark masses exist [15,64], we have begun two flavor domain wall fermion calculations [19,20,65], and $2 + 1$ flavor domain wall fermion calculations are just beginning. These studies begin to address the quenching error. In addition, systematic uncertainties due to continuum, chiral and infinite volume extrapolations must be addressed as in the extensive quenched study using improved Wilson fermions reported in [25]. This study suggests domain wall fermions should facilitate these extrapolations. Recent results from chiral perturbation theory [66,67] may also prove useful.

ACKNOWLEDGMENTS

We thank our colleagues in the RBC collaboration, Y. Aoki, C. Dawson, N. Christ, T. Izubuchi, C. Jung, R. Mawhinney, and A. Soni for useful and stimulating discussions. K. O. also thanks M. Savage for helpful suggestions on the text. The numerical computations reported here were done on the 400 Gflops QCDSP supercomputer [68] at Columbia University and the 600 Gflops QCDSP supercomputer [69] at the RIKEN BNL Research Center. We thank RIKEN, Brookhaven National Laboratory and the U.S. Department of Energy for providing the facilities essential for the completion of this work. This research was supported in part by the RIKEN BNL Research Center and in part by DOE grant No. DF-FC02-94ER40818 (Orginos).

[1] M. Breidenbach *et al.*, Phys. Rev. Lett. **23**, 935 (1969).
[2] J. I. Friedman, Rev. Mod. Phys. **63**, 615 (1991).
[3] H. W. Kendall, Rev. Mod. Phys. **63**, 597 (1991).
[4] R. E. Taylor, Rev. Mod. Phys. **63**, 573 (1991).
[5] M. Gluck, E. Reya, M. Stratmann, and W. Vogelsang, Phys. Rev. D **53**, 4775 (1996).
[6] T. Gehrmann and W. J. Stirling, Phys. Rev. D **53**, 6100 (1996).
[7] H. L. Lai *et al.*, Phys. Rev. D **55**, 1280 (1997).
[8] D. Adams *et al.* (Spin Muon (SMC)), Phys. Rev. D **56**, 5330 (1997).
[9] B. Adeva *et al.* (Spin Muon), Phys. Lett. B **420**, 180 (1998).
[10] M. Gluck, E. Reya, and A. Vogt, Eur. Phys. J. C **5**, 461 (1998).
[11] K. Ackerstaff *et al.* (HERMES), Phys. Lett. B **464**, 123 (1999).
[12] A. D. Martin, R. G. Roberts, W. J. Stirling, and R. S. Thorne, Eur. Phys. J. C **23**, 73 (2002).
[13] M. Gockeler *et al.*, Phys. Rev. D **53**, 2317 (1996).
[14] M. Gockeler *et al.*, hep-ph/9909253.
[15] D. Dolgov *et al.* (LHPC), Phys. Rev. D **66**, 034506 (2002).
[16] M. Gockeler, R. Horsley, D. Pleiter, P. E. L. Rakow, and G. Schierholz, Nucl. Phys. B, Proc. Suppl. **119**, 32 (2003).
[17] K. Orginos (RBC), Nucl. Phys. B, Proc. Suppl. **106**, 721 (2002).
[18] P. Hagler *et al.* (LHPC), Phys. Rev. D **68**, 034505 (2003).
[19] S. Ohta and K. Orginos (RBCK), Nucl. Phys. B, Proc. Suppl. **129**, 296 (2004).
[20] S. Ohta and K. Orginos (RBCK), Nucl. Phys. B, Proc. Suppl. **140**, 396 (2005).
[21] S. Sasaki, K. Orginos, S. Ohta, and T. Blum (RIKEN-BNL-Columbia-KEK), Phys. Rev. D **68**, 054509 (2003).
[22] LHPC, Phys. Rev. Lett. **93**, 112001 (2004).

[23] M. Gockeler *et al.* (QCDSF), Phys. Rev. Lett. **92**, 042002 (2004).
[24] A. A. Khan *et al.*, Nucl. Phys. B, Proc. Suppl. **140**, 408 (2005).
[25] M. Gockeler, R. Horsley, D. Pleiter, P. E. L. Rakow, and G. Schierholz (QCDSF), Phys. Rev. D **71**, 114511 (2005).
[26] W. Detmold, W. Melnitchouk, J. W. Negele, D. B. Renner, and A. W. Thomas, Phys. Rev. Lett. **87**, 172001 (2001).
[27] D. B. Kaplan, Phys. Lett. B **288**, 342 (1992).
[28] Y. Shamir, Nucl. Phys. **B406**, 90 (1993).
[29] V. Furman and Y. Shamir, Nucl. Phys. **B439**, 54 (1995).
[30] K. Orginos (RBC), Nucl. Phys. B, Proc. Suppl. **106**, 721 (2002).
[31] Y. Aoki *et al.*, Phys. Rev. D **69**, 074504 (2004).
[32] M. Gockeler *et al.*, Phys. Rev. D **54**, 5705 (1996).
[33] R. L. Jaffe and X.-D. Ji, Phys. Rev. Lett. **67**, 552 (1991).
[34] R. L. Jaffe and X.-D. Ji, Nucl. Phys. **B375**, 527 (1992).
[35] V. Barone, A. Drago, and P. G. Ratcliffe, Phys. Rep. **359**, 1 (2002).
[36] S. Sasaki, T. Blum, and S. Ohta, Phys. Rev. D **65**, 074503 (2002).
[37] G. Martinelli and C. T. Sachrajda, Nucl. Phys. **B316**, 355 (1989).
[38] M. Gockeler *et al.*, Phys. Rev. D **63**, 074506 (2001).
[39] J. E. Mandula, G. Zweig, and J. Govaerts, Nucl. Phys. **B228**, 109 (1983).
[40] G. Martinelli, C. Pittori, C. T. Sachrajda, M. Testa, and A. Vladikas, Nucl. Phys. **B445**, 81 (1995).
[41] T. Blum *et al.*, Phys. Rev. D **66**, 014504 (2002).
[42] C. Dawson *et al.* (RBC), Nucl. Phys. B, Proc. Suppl. **119**, 314 (2003).
[43] M. Gockeler *et al.*, Nucl. Phys. **544**, 699 (1999).
[44] J. A. Gracey, Nucl. Phys. **B662**, 247 (2003).
[45] A. J. Buras, hep-ph/9806471.
[46] V. Gimenez, L. Giusti, F. Rapuano, and M. Talevi, Nucl. Phys. **B531**, 429 (1998).
[47] S. Capitani, M. Luscher, R. Sommer, and H. Wittig (ALPHA), Nucl. Phys. **B544**, 669 (1999).
[48] T. Takaishi, Phys. Rev. D **54**, 1050 (1996).
[49] P. de Forcrand *et al.* (QCD-TARO), Nucl. Phys. **B577**, 263 (2000).
[50] D. Arndt and M. J. Savage, Nucl. Phys. A **697**, 429 (2002).
[51] J.-W. Chen and M. J. Savage, Nucl. Phys. A **707**, 452 (2002).
[52] J. Blumlein, H. Bottcher, and A. Guffanti, Nucl. Phys. B, Proc. Suppl. **135**, 152 (2004).
[53] M. Gurtler *et al.*, Nucl. Phys. B, Proc. Suppl. **140**, 707 (2005).
[54] J.-W. Chen and X.-d. Ji, Phys. Lett. B **523**, 107 (2001).
[55] W. Detmold, W. Melnitchouk, and A. W. Thomas, Int. J. Mod. Phys. A **18**, 1343 (2003).
[56] W. Detmold, W. Melnitchouk, and A. W. Thomas, Phys. Rev. D **66**, 054501 (2002).
[57] A. W. Thomas, Nucl. Phys. B, Proc. Suppl. **119**, 50 (2003).
[58] S. Wandzura and F. Wilczek, Phys. Lett. B **72**, 195 (1977).
[59] R. L. Jaffe and X.-D. Ji, Phys. Rev. D **43**, 724 (1991).
[60] B. Surrow (STAR), hep-ex/0205090.
[61] L. C. Bland (STAR), hep-ex/0403012.
[62] M. Gockeler *et al.* (QCDSF), Nucl. Phys. **A755**, 537 (2005).
[63] J.-W. Chen and X.-d. Ji, Phys. Rev. Lett. **87**, 152002 (2001).
[64] M. Gockeler *et al.* (QCDSF), Nucl. Phys. B, Proc. Suppl. **140**, 399 (2005) .
[65] Y. Aoki *et al.*, Phys. Rev. D **72**, 114505 (2005).
[66] S. R. Beane and M. J. Savage, Phys. Rev. D **68**, 114502 (2003).
[67] W. Detmold and C. J. D. Lin, Phys. Rev. D **71**, 054510 (2005).
[68] D. Chen *et al.*, Nucl. Phys. B, Proc. Suppl. **73**, 898 (1999).
[69] R. D. Mawhinney, Parallel Computing **25**, 1281 (1999).